The 9th European Congress on Computational Methods in Applied Sciences and Engineering
ECCOMAS Congress 2024
3–7 June 2024, Lisboa, Portugal

ADAPTIVELY TUNED HIGH-ORDER METHODS FOR ILES

Panagiotis Tsoutsanis[1], Lin Fu[2], Xesus Nogueira[3]

[1] Centre for Computational Engineering Sciences
Cranfield University
Cranfield MK43 0AL, United Kingdom
e-mail: panagiotis.tsoutsanis@cranfield.ac.uk

[2] Department of Mechanical and Aerospace Engineering
The Hong Kong University of Science and Technology
Clear Water Bay, Kowloon, Hong Kong
email: linfu@ust.hk

[3]Group of Numerical Methods in Engineering-GMNI
Center for Technological Innovation in Construction and Civil Engineering-CITEEC
Universidade da Coruña, Campus de Elviña, 15071, A Coruña, Spain
email:xesus.nogueira@udc.es

Key words: CFD, iLES, High-Order Finite-Volume, CWENOZ

Summary. Implicit Large Eddy Simulation (iLES) is popular for modeling high-Reynolds-number turbulent flows due to its simplicity and efficiency. High-resolution numerical schemes in iLES mimic subgrid-scale models by using numerical dissipation/dispersion errors. Balancing these errors is crucial to avoid unphysical energy build-up or excessive diffusion, especially in compressible flows with discontinuities and smooth features. This work introduces an adaptive dissipation/dispersion adjustment (ADDA) algorithm for the CWENOZ scheme in a finite-volume framework for unstructured meshes, tested in subsonic, transonic, and supersonic regimes. The ADDA algorithm enhances robustness and scale-resolving capabilities, yielding efficient and physically meaningful results, and is available in the open-source UCNS3D CFD solver.

1 INTRODUCTION

Turbulent flows with high Reynolds number feature a wide range of spatial and temporal scales that present significant challenges for their numerical simulation. The smaller flow scales are often too fine for the grid resolution of numerical methods. This mismatch leads to under-resolved flows, where small scales can't be accurately captured, affecting the overall dynamics of the flow. Direct numerical simulation (DNS) of such flows is computationally impractical, even with advanced supercomputers. Instead, Large Eddy Simulation (LES) methods are used, which resolve larger scales and model the effects of smaller, unresolved scales with subgrid-scale (SGS) models. Implicit LES (iLES) incorporates the effects of unresolved scales implicitly through the inherent numerical dissipation of high-resolution, non-oscillatory methods, eliminating the need for explicit SGS models. iLES is widely adopted in numerical frameworks like finite-volume (FV), finite-element (FE), finite-difference (FD), and various high-order schemes such as WENO, MUSCL, and TVD [1–7]. High-resolution schemes naturally introduce numerical

dissipation that mimics SGS models, and they should balance low numerical dissipation and dispersion, avoiding unphysical energy build-up in high modes, especially in under-resolved grids. This balance ensures that the energy transfer from larger to smaller scales, truncated in practical computations, is effectively dissipated at the smallest scales present. This work focuses on adapting numerical methods to provide the right amount of dissipation for iLES simulations, minimizing unphysical energy build-up in high modes. Various approaches address this [1, 3, 8–14], such as polynomial de-aliasing techniques, adaptive dissipation blending, and multi-objective optimization. Automatic dissipation adjustment methods adjust dissipation based on energy ratios, maintaining stability even in compressible flows with potential shock waves. We develop an a priori approach for adaptively adjusting dissipation and dispersion (ADDA) in high-order non-oscillatory methods for unstructured meshes, suitable for practical engineering problems. We employ well established test problems, such as the Taylor-Green vortex and the turbulent flow past the SD7003 airfoil to demonstrate the performance of the new framework. The chosen numerical scheme is the high-order CWENOZ method [2] , implemented in the UCNS3D CFD code [15] using Fortran 2008, MPI, and OpenMP [16].

2 NUMERICAL FRAMEWORK

2.1 Governing Equations

The compressible Navier-Stokes equations are considered, written in conservative form as:

$$\frac{\partial \mathbf{U}(\mathbf{x},t)}{\partial t} + \nabla \cdot (\vec{\mathbf{F}}_c(\mathbf{U}) - \vec{\mathbf{F}}_v(\mathbf{U}, \nabla \mathbf{U})) = 0, \tag{1}$$

where $\mathbf{U}$ is the vector of the conserved variables, $\vec{\mathbf{F}}_c$ and $\vec{\mathbf{F}}_v$ are the inviscid and viscous flux vectors, respectively, as

$$\mathbf{U} = \begin{bmatrix} \rho \\ \rho u \\ \rho v \\ \rho w \\ E \end{bmatrix}, \vec{\mathbf{F}}_c = \begin{bmatrix} \rho u_n \\ \rho u u_n + n_x p \\ \rho v u_n + n_y p \\ \rho w u_n + n_z p \\ u_n(E+p) \end{bmatrix}, \vec{\mathbf{F}}_v = \begin{bmatrix} 0 \\ n_x\tau_{xx} + n_y\tau_{xy} + n_z\tau_{xz} \\ n_x\tau_{yx} + n_y\tau_{yy} + n_z\tau_{yz} \\ n_x\tau_{zx} + n_y\tau_{zy} + n_z\tau_{zz} \\ n_x\Theta_x + n_y\Theta_y + n_z\Theta_z \end{bmatrix}, \tag{2}$$

where ρ is the density; u, v, w are the velocity components in x, y and z Cartesian coordinates, respectively, and u_n is the velocity normal to the bounded surface area, defined by $u_n = n_x u + n_y v + n_z w$. The total energy per unit mass is given by $E = p/(\gamma - 1) + (1/2)\rho(u^2 + v^2 + w^2)$, where p is the pressure, $\gamma = 1.4$ is the ratio of specific heats for air at normal atmospheric conditions, and the Sutherland's law is assumed. The viscous stresses and heat conduction, Θ, is given by:

$$\begin{aligned} \Theta_x &= u\tau_{xx} + v\tau_{xy} + w\tau_{xz} + \frac{\mu_l}{Pr}\frac{\gamma}{(\gamma-1)}\frac{\partial T}{\partial x}, \\ \Theta_y &= u\tau_{yx} + v\tau_{yy} + w\tau_{yz} + \frac{\mu_l}{Pr}\frac{\gamma}{(\gamma-1)}\frac{\partial T}{\partial y}, \\ \Theta_z &= u\tau_{zz} + v\tau_{zy} + w\tau_{zz} + \frac{\mu_l}{Pr}\frac{\gamma}{(\gamma-1)}\frac{\partial T}{\partial z}. \end{aligned} \tag{3}$$

The viscous stress tensor τ_{ij} is defined by is

$$\tau_{ij} = \mu_l \left(\frac{\partial \mathbf{u}_i}{\partial \mathbf{x}_j} + \frac{\partial \mathbf{u}_j}{\partial \mathbf{x}_i} - \frac{2}{3} \frac{\partial \mathbf{u}_k}{\partial \mathbf{x}_k} \delta_{ij} \right), \tag{4}$$

where δ_{ij} is the Kronecker delta and the subscripts i, j, k refer to the Cartesian coordinate components $\mathbf{x} = (x, y, z)$.

2.2 CWENOZ Discretisation

We discretise the Navier-Stokes on a 3D domain Ω consisting of any combination of conforming tetrahedral, hexahedral, prism or pyramids in 3D, by integrating Eq. (1) over each mesh element i using a high-order explicit finite-volume formulation the following equation is obtained:

$$\begin{aligned} \frac{d\mathbf{U}_i}{dt} = &- \frac{1}{|V_i|} \sum_{l=1}^{N_f} \sum_{\alpha=1}^{N_{qp}} \vec{\mathbf{F}}_{c_l} \left(\mathbf{U}^n_{l,L}(\mathbf{x}_{l,\alpha}, t), \mathbf{U}^n_{l,R}(\mathbf{x}_{l,\alpha}, t) \right) \omega_\alpha |S_l| \\ &+ \frac{1}{|V_i|} \sum_{l=1}^{N_f} \sum_{\alpha=1}^{N_{qp}} \vec{\mathbf{F}}_{v_l} \left(\mathbf{U}^n_{l,L}(\mathbf{x}_{l,\alpha}, t), \mathbf{U}^n_{l,R}(\mathbf{x}_{l,\alpha}, t), \nabla \mathbf{U}^n_{l,L}(\mathbf{x}_{l,\alpha}, t), \nabla \mathbf{U}^n_{l,R}(\mathbf{x}_{l,\alpha}, t) \right) \omega_\alpha |S_l|, \end{aligned} \tag{5}$$

where $\mathbf{U}_i$ are the volume averaged conserved variables

$$\mathbf{U}_i = \frac{1}{|V_i|} \int_{V_i} \mathbf{U}(x, y, z)\, dV, \tag{6}$$

and $\vec{\mathbf{F}}_{c_l}$ and $\vec{\mathbf{F}}_{v_l}$ are the numerical flux function, N_{qp} is the number of quadrature points, N_f is the number of faces, , $|S_l|$ is the surface area , and $\mathbf{U}^n_{l,L}(\mathbf{x}_{l,\alpha}, t)$ and $\mathbf{U}^n_{l,R}(\mathbf{x}_{l,\alpha}, t)$ are the boundary extrapolated reconstructed solutions for the left and right side of the interface, $\nabla \mathbf{U}^n_{l,L}(\mathbf{x}_{l,\alpha}, t)$ and $\nabla \mathbf{U}^n_{l,R}(\mathbf{x}_{l,\alpha}, t)$ are the the gradients for the left and right side of the interface; while α corresponds to different Gaussian integration points $\mathbf{x}_\alpha$ and weights ω_α over each face. We employ the CWENOZ scheme of Tsoutsanis and Dumbser [2], and only the key components are presented in this work. The CWENOZ scheme combines an optimal (high-order) p_{opt} polynomial from the central stencil with lower-order polynomials from directional stencils.The definition of an optimal polynomial given by:

$$p_{opt}(x, y, z) = \sum_{s=1}^{s_t} \lambda_s p_s(z, y, z), \tag{7}$$

where s is the stencil index, with $s = 1$ being the central, $s = (2, 3, .., s_t)$ being the directional, s_t being the total number of stencils, and λ_s being the linear coefficient for each stencil, whose sum is equal to 1. The p_1 polynomial is computed by subtracting the lower-order polynomials from the optimum polynomial as follows:

$$p_1(x, y, z) = \frac{1}{\lambda_1} \left(p_{opt}(x, y, z) - \sum_{s=2}^{s_t} \lambda_s p_s(x, y, z) \right). \tag{8}$$

The CWENOZ reconstruction polynomial is a non-linear combination of all the polynomials as follows:

$$p(x,y,z)^{\text{cwenoz}} = \sum_{s=1}^{s_t} \omega_s p_s(x,y,z) \equiv \mathbf{U}_0 + \sum_{k=1}^{K} \tilde{a}_k \phi_k(x,y,z), \tag{9}$$

where ω_s corresponds to the non-linear weights assigned to each reconstruction polynomial, and $\tilde{a}_k$ are the reconstructed degrees of freedom; and the non-linear weight ω_s is defined as: The non-linear weights are now defined as:

$$\omega_s = \frac{\tilde{\omega}_s}{\sum_{s=1}^{s_t} \tilde{\omega}_s} \quad \text{where} \quad \tilde{\omega}_s = \lambda_s \left(1 + \left(\frac{\tau}{\epsilon + \mathcal{SI}_s}\right)^b\right). \tag{10}$$

With τ being the universal oscillation indicator and taken as the absolute difference between the smoothness indicators as follows:

$$\tau = \left(\frac{\sum_{s=2}^{s_t} |\mathcal{SI}_s - \mathcal{SI}_1|}{s_t - 1}\right). \tag{11}$$

The linear weight of the central stencil is assigned an arbitrary large value and the directional stencils an equal value, and then their values are normalised with their sum being equal to unitu. For the definitions of smoothness indicator the reader is referred to [2], and the reader is referred to [**?**, 17–26] and references therein regarding the implementation.

2.3 Time Advancement & Fluxes

We employ the explicit 4th-order Strong-Stability-Preserving (SSP) Runge-Kutta of Spiteri and Ruuth [27],[27] or the widely used dual-time stepping strategy [28] in an implicit matrix-free lower-upper symmetric Gauss-Seidel (LU-SGS) fashion [29, 30] using the Rusanov flux [31] as detailed in implementation [15] and references therein. For the inviscid fluxes we employ the Roe Riemann solver [32] and for the viscous fluxes, the gradients are computed using a constrained least-square reconstruction for the boundary condition enforcement including penalty terms as detailed in [15, 21] and references therein.

2.4 ADDA

From of the flow-chart of the `ADDA`-augmented `UCNS3D` code as shown in Fig. 1 at every physical time step for every cell three steps are taken. Firstly we measure the Energy Ratio as defined in [1], to establish if the field of that cell is well-resolved or under-resolved, and in turn dictates if this cell requires more or less dissipation. The 2nd step is involved the adaptation of CWENOZ reconstruction by adjusting the linear weight (λ_1) of the central high-order stencil. The third step involves the flux adaptation be adjusting the dissipation (gradual increase, gradual decrease, or return to default value) through a flux dissipation control term (d_i) that is multiplied with each of the wave strengths of the Roe Riemann solver, depending on the value of the non-linear CWENOZ weight for the density and pressure, to ensure that the non-oscillatory properties of the framework are maintained. Finally, the fluxes are computed, and the solution advanced in time.

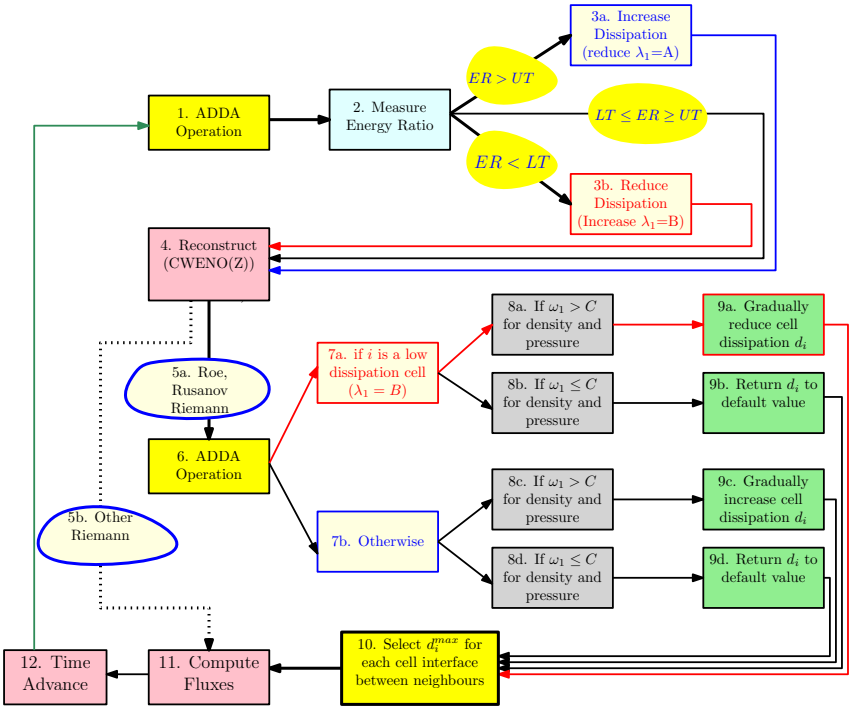

Figure 1: ADDA flow chart

3 RESULTS

3.1 Taylor-Green Vortex

The iLES of the 3D inviscid subsonic Taylor-Green vortex test problem is employed for assessing the performance of the developed schemes, as it is widely used by the community for this reason [1, 5, 33–41] and therefore there is a wealth of DNS, LES, iLES computational data from the literature to compare against, and the readers are referred to the work of [33] for the initial conditions for this flow problem. We are interested in coarse grid resolutions, being more representative of the operating conditions of high-order methods, to better understand any benefits that the new `ADDA` technique can offer for reproducing the transition to turbulence in these situations. The computational domain is defined as $\Omega = [0, 2\pi]^3$ with periodic boundary conditions and the initial condition corresponds to an initial Mach number $M \approx 0.08$, with wavenumber $k = 2\pi/\lambda = 1$. Simulations were carried out on hexahedral meshes of 64^3 and 128^3. For the present Taylor-Green vortex flow test problem we employ the CWENOZ 5th-order scheme and the 4th-order Runge-Kutta SSP with a CFL of 1.4, with the Roe Riemann solver. We are assess the performance of the newly introduced framework by examining the kinetic energy temporal evolution, dissipation rate, and 3D spectra of the kinetic energy after the dissipation peak ($t = 10$). It can be noticed from Fig. 2 that the ADDA variants provide a better agreement with DNS results of Brachet [33] and the theoretical Kolmogorov's slope at both resolutions although several cells were required to increased their dissipation term as shown in Fig. 3.

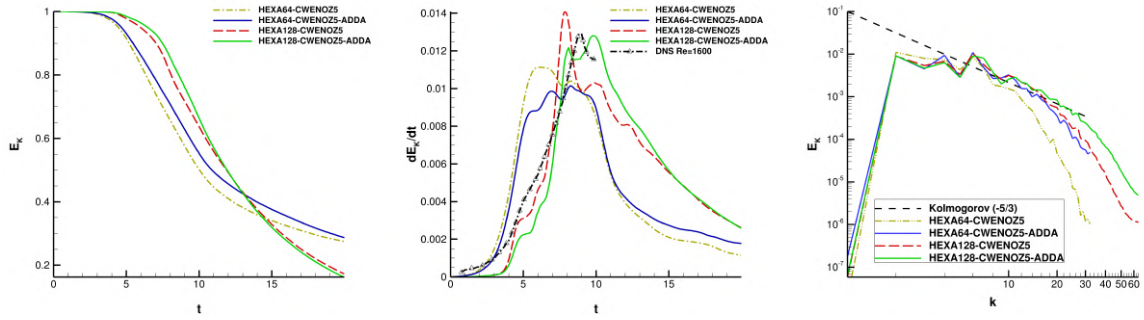

Figure 2: Kinetic energy (left), kinetic energy dissipation rate(middle), and kinetic energy spectra at t=10 for the inviscid Taylor Green vortex using various schemes.

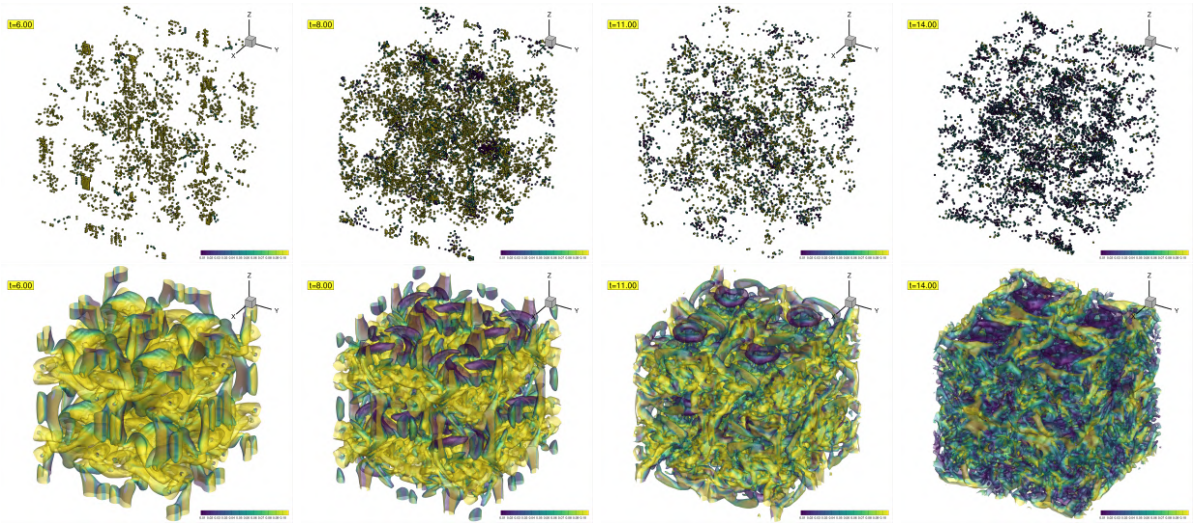

Figure 3: Cells identified for increased dissipation for the Taylor-Green vortex flow problem at different instants (top), and iso-surfaces of Q-criterion coloured by kinetic energy (bottom) using a CWENOZ5-ADDA scheme.

3.2 SD7003

We apply the developed framework to the turbulent flow over the SD7003 wing at Mach number of $M = 0.2$, at Reynolds number $Re = 60,000$ and angle of attack of $\alpha = 8°$. This benchmark case has been widely used to assess the performance of LES methods [37,42–45]. For this purpose we employ the CWENOZ4-ADDA scheme on a hybrid unstructured mesh consisting of 5.3 million cells as illustrated in Fig. 4. The domain extends $50c$ upstream and downstream, and $0.2c$ in the span-wise direction, where c is the chord length. The grid resolution at the boundary layer region gives a ($y^+ = 0.87$,$x^+ = 3.1$,$z^+ = 5.4$) with no-slip boundary conditions at the surface of the aerofoil, free-stream conditions at the farfield and periodic boundary conditions in the span-wise direction. All the schemes employ the low-Mach number correction [45], the Roe Riemann solver [32] and the 2nd-order implicit dual-time stepping available in `UCNS3D` [15] with a timestep size of $\Delta t = \frac{t_c}{500}$ with the convection time being given by $t_c = c/U_\infty$. The

simulations were run for $t = 20t_c$ to develop the flow, and an additional $20t_c$ for time averaging. It can be noticed from Fig. 5 and Fig. 6 that the ADDA variant provides the correct predictions, and is in good agreement with previous computational studies in terms of lift, drag, separation and reattachment locations as seen in Table 1. More importantly we notice that the cells in the laminar region at the wake have been adjusted for reduced dissipation since these are well resolved regions, while in the transitional region they are tagged for high dissipation.

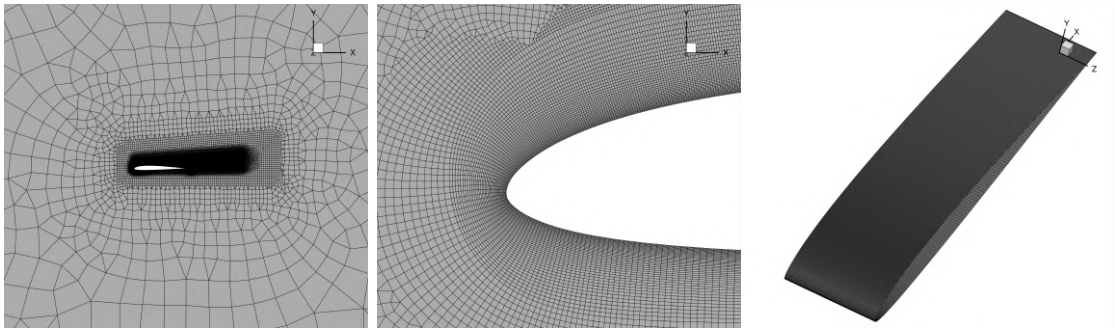

Figure 4: Unstructured mesh used for the SD7003 airfoil test problem.

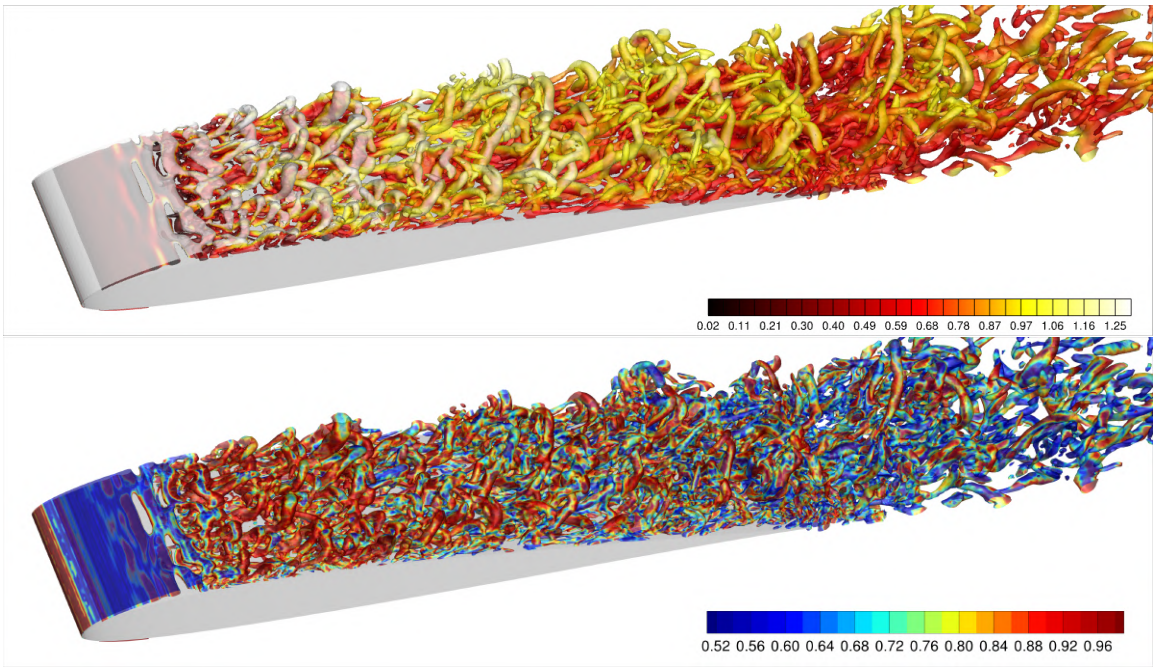

Figure 5: Instantaneous iso-surfaces of Q criterion (Q=100) coloured by the non-dimensionalised velocity magnitude (top) and the `ADDA` flux dissipation d_i for the SD7003 airfoil with the CWENOZ4-`ADDA` scheme. The LSB is characterised by a low-dissipation d_i value and a high-dissipation profile in the turbulent region according to the energy ratio values.

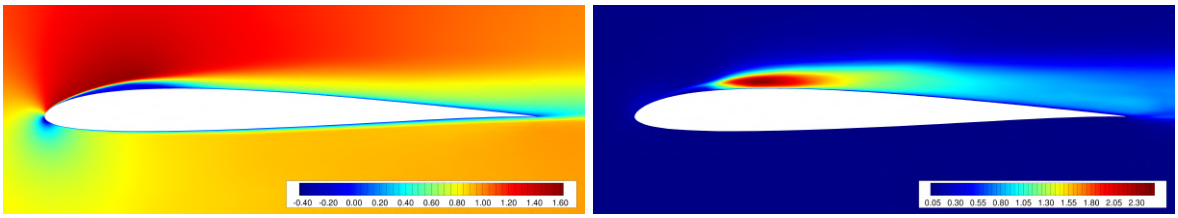

Figure 6: Time-averaged, span-wise averaged contour plots of non-dimensional u-velocity (left) and turbulent kinetic energy (right) for the SD7003 flow problems with `CWENOZ4-ADDA`.

Method	C_L	C_D	x_s	x_r
CWENOZ4-ADDA-mesh	0.927	0.045	0.041	0.270
Frank et al. [43]	0.923	0.045	0.027	0.310
Galbraith & Visbal [46]	0.917	0.044	0.031	0.303

Table 1: Predictions for lift-coefficient C_L, drag-coefficient C_D, separation position x_s, and reattachment position x_r for the SD7003 airfoil test problem and comparison with computational studies in the literature.

4 CONCLUSIONS

This work developed an adaptive dissipation/dispersion adjustment algorithm within a high-order finite-volume framework for iLES simulations of compressible turbulent flows. The algorithm measures the energy ratio to adjust the CWENOZ reconstruction and the dissipation term of the Roe Riemann solver for each cell at each time step. It was tested on several problems, showing improved scale-resolving capability and non-oscillatory properties. The algorithm's versatility suggests potential applications in other frameworks like DG and hybrid DG-FV.

5 ACKNOWLEDGEMENTS

P.T. acknowledges the computing time on ARCHER2 through UK Turbulence Consortium by the EPSRC grant [EP/X035484/1] and the support by the EPSRC grant [EP/W037092/1]. L.F. acknowledges the fund from the Research Grants Council (RGC) of the Government of Hong Kong Special Administrative Region (HKSAR) with RGC/ECS Project (No. 26200222), RGC/GRF Project (No. 16201023) and RGC/STG Project (No. STG2/E-605/23-N), the fund from Guangdong Basic and Applied Basic Research Foundation (No. 2024A1515011798), and the fund from Guangdong Province Science and Technology Plan Project (No. 2023A0505030005). X.N. acknowledges the support provided by the [Grant PID2021-125447OB-I00] funded by MCIN/AEI/ 10.13039/501100011033 and by "ERDF A way of making Europe", the funds by [Grant TED2021-129805B-I00] funded by MCIN/AEI/ 10.13039/501100011033 and by the "European Union NextGenerationEU/PRTR" and the funding provided by the Xunta de Galicia [Grant #ED431C 2022/06].

REFERENCES

[1] J. Fernandez-Fidalgo, L. Ramirez, P. Tsoutsanis, I. Colominas, X. Nogueira, A reduced-dissipation WENO scheme with automatic dissipation adjustment, Journal of

Computational Physics 425 (2021). doi:10.1016/j.jcp.2020.109749.

[2] P. Tsoutsanis, M. Dumbser, Arbitrary high order central non-oscillatory schemes on mixed-element unstructured meshes, Computers and Fluids 225 (2021). doi:10.1016/j.compfluid.2021.104961.

[3] D. Flad, A. Beck, C. Munz, Simulation of underresolved turbulent flows by adaptive filtering using the high order discontinuous Galerkin spectral element method, Journal of Computational Physics 313 (2016) 1–12.

[4] J. Domaradzki, K. Loh, P. Yee, Large eddy simulations using the subgrid-scale estimation model and truncated Navier-Stokes dynamics, Theoretical and Computational Fluid Dynamics 15 (6) (2002) 421–450.

[5] D. Drikakis, C. Fureby, F. Grinstein, D. Youngs, Simulation of transition and turbulence decay in the Taylor-Green vortex, Journal of Turbulence 8 (2007) 1–12.

[6] X. Nogueira, L. Cueto-Felgueroso, I. Colominas, H. Gomez, Implicit large eddy simulation of non-wall-bounded turbulent flows based on the multiscale properties of a high-order finite volume method, Computer Methods in Applied Mechanics and Engineering 199 (9-12) (2010) 615–624. doi:10.1016/j.cma.2009.10.013.

[7] A. Uranga, P.-O. Persson, M. Drela, J. Peraire, Implicit large eddy simulation of transition to turbulence at low Reynolds numbers using a discontinuous Galerkin method, International Journal for Numerical Methods in Engineering 87 (1-5) (2011) 232–261. doi:10.1002/nme.3036.

[8] J. Domaradzki, Effective eddy viscosities in implicit modeling of decaying high Reynolds number turbulence with and without rotation, Fluid Dynamics Research 36 (4-6) (2005) 385–406.

[9] T. Tantikul, J. Domaradzki, Large eddy simulations using truncated Navier-Stokes equations with the automatic filtering criterion, Journal of Turbulence 11 (2010) 1–24.

[10] S. Hickel, N. Adams, J. Domaradzki, An adaptive local deconvolution method for implicit LES, Journal of Computational Physics 213 (1) (2006) 413–436. doi:https://doi.org/10.1016/j.jcp.2005.08.017.

[11] X. Nogueira, L. Ramirez, J. Fernandez-Fidalgo, M. Deligant, S. Khelladi, J.-C. Chassaing, F. Navarrina, An a posteriori-implicit turbulent model with automatic dissipation adjustment for large eddy simulation of compressible flows, Computers and Fluids 197 (2020). doi:10.1016/j.compfluid.2019.104371.

[12] A. R. Winters, R. C. Moura, G. Mengaldo, G. J. Gassner, S. Walch, J. Peiro, S. J. Sherwin, A comparative study on polynomial dealiasing and split form discontinuous Galerkin schemes for under-resolved turbulence computations, Journal of Computational Physics 372 (2018) 1–21. doi:10.1016/j.jcp.2018.06.016.

[13] T. Liang, L. Fu, Finite-volume teno scheme with a new cell-interface flux evaluation strategy for unstructured meshes, Communications in Computational Physics 35 (4) (2024) 938–972. doi:https://doi.org/10.4208/cicp.OA-2023-0289.

[14] D. Yuan, K. Jenkins, P. Tsoutsanis, Numerical investigation of the inviscid taylor-green vortex using an adaptive filtering method for a modal discontinuous galerkin method, International Journal of Computational Fluid Dynamics 37 (2023) 522–540. doi:doi.org/10.1080/10618562.2024.2329775.

[15] A. Antoniadis, D. Drikakis, P. Farmakis, L. Fu, I. Kokkinakis, X. Nogueira, P. Silva, M. Skote, V. Titarev, P. Tsoutsanis, UCNS3D: An open-source high-order finite-volume unstructured CFD solver, Computer Physics Communications 279 (2022). doi:10.1016/j.cpc.2022.108453.

[16] P. Tsoutsanis, A. Antoniadis, K. Jenkins, Improvement of the computational performance of a parallel unstructured WENO finite volume cfd code for implicit large eddy simulation, Computers and Fluids 173 (2018) 157–170. doi:10.1016/j.compfluid.2018.03.012.

[17] V. Maltsev, M. Skote, P. Tsoutsanis, High-order hybrid DG-FV framework for compressible multi-fluid problems on unstructured meshes, Journal of Computational Physics 502 (2024) 112819. doi:doi.org/10.1016/j.jcp.2024.112819.

[18] P. Tsoutsanis, E. Adebayo, A. Merino, A. Arjona, M. Skote, CWENO finite-volume interface capturing schemes for multicomponent flows using unstructured meshes, Journal of Scientific Computing 89 (3) (2021). doi:10.1007/s10915-021-01673-y.

[19] P. Tsoutsanis, M. Pavan Kumar, P. Farmakis, A relaxed a posteriori MOOD algorithm for multicomponent compressible flows using high-order finite-volume methods on unstructured meshes, Applied Mathematics and Computation 437 (2023). doi:10.1016/j.amc.2022.127544.

[20] E. M. Adebayo, P. Tsoutsanis, K. W. Jenkins, Application of central-weighted essentially non-oscillatory finite-volume interface-capturing schemes for modeling cavitation induced by an underwater explosion, Fluids 9 (2) (2024). doi:10.3390/fluids9020033.

[21] P. Tsoutsanis, A. Antoniadis, D. Drikakis, WENO schemes on arbitrary unstructured meshes for laminar, transitional and turbulent flows, Journal of Computational Physics 256 (2014) 254–276. doi:10.1016/j.jcp.2013.09.002.

[22] P. Tsoutsanis, V. Titarev, D. Drikakis, WENO schemes on arbitrary mixed-element unstructured meshes in three space dimensions, Journal of Computational Physics 230 (4) (2011) 1585–1601. doi:10.1016/j.jcp.2010.11.023.

[23] P. Silva, P. Tsoutsanis, A. Antoniadis, Simple multiple reference frame for high-order solution of hovering rotors with and without ground effect, Aerospace Science and Technology 111 (2021). doi:10.1016/j.ast.2021.106518.

[24] P. Farmakis, P. Tsoutsanis, X. Nogueira, WENO schemes on unstructured meshes using a relaxed a posteriori MOOD limiting approach, Computer Methods in Applied Mechanics and Engineering 363 (2020). doi:10.1016/j.cma.2020.112921.

[25] P. Tsoutsanis, Extended bounds limiter for high-order finite-volume schemes on unstructured meshes, Journal of Computational Physics 362 (2018) 69–94. doi:10.1016/j.jcp.2018.02.009.

[26] A. Antoniadis, P. Tsoutsanis, D. Drikakis, Assessment of high-order finite volume methods on unstructured meshes for rans solutions of aeronautical configurations, Computers and Fluids 146 (2017) 86–104. doi:10.1016/j.compfluid.2017.01.002.

[27] R. J. Spiteri, S. J. Ruuth, A new class of optimal high-order strong-stability-preserving time-stepping schemes, SIAM Journal of Numerical Analysis 40 (2) (2002) 469–491.

[28] A. Jameson, Time dependent calculations using multigrid, with applications to unsteady flows past airfoils and wings, AIAA paper 6 (1991-1596) (1991). doi:https://doi.org/10.2514/6.1991-1596.

[29] H. Luo, J. Baum, R. Lohner, A fast, matrix-free implicit method for compressible flows on unstructured grids, Journal of Computational Physics 146 (2) (1998) 664–690.

[30] M. Petrov, A. Tambova, V. Titarev, S. Utyuzhnikov, A. Chikitkin, Flowmodellium software package for calculating high-speed flows of compressible fluid, Comput. Math. & Math. Phys. 58 (11) (2018) 1865–1886.

[31] V. Rusanov, The calculation of the interaction of non-stationary shock waves and obstacles, USSR Computational Mathematics and Mathematical Physics 1 (1962) 304–320. doi:10.1016/0041-5553(62)90062-9.

[32] P. Roe, Approximate riemann solvers, parameter vectors, and difference schemes, Journal of Computational Physics 43 (2) (1981) 357–372. doi:10.1016/0021-9991(81)90128-5.

[33] M. Brachet, D. Meiron, B. Nickel, R. Morf, U. Frisch, S. Orszag, Small-scale structure of the Taylor-Green vortex, Journal of Fluid Mechanics 130 (1983) 411–452. doi:10.1017/S0022112083001159.

[34] J. Bull, A. Jameson, Simulation of the Taylor-Green vortex using high-order flux reconstruction schemes, AIAA Journal 53 (9) (2015) 2750–2761.

[35] C.-W. Shu, W.-S. Don, D. Gottlieb, O. Schilling, L. Jameson, Numerical convergence study of nearly incompressible, inviscid Taylor-Green vortex flow, Journal of Scientific Computing 24 (1) (2005) 569–595.

[36] C.-G. Li, M. Tsubokura, An implicit turbulence model for low-Mach Roe scheme using truncated Navier-Stokes equations, Journal of Computational Physics 345 (2017) 462–474. doi:https://doi.org/10.1016/j.jcp.2017.05.032.

[37] B. Vermeire, P. Vincent, On the properties of energy stable flux reconstruction schemes for implicit large eddy simulation, Journal of Computational Physics 327 (2016) 368–388.

[38] L. Fu, A very-high-order TENO scheme for all-speed gas dynamics and turbulence, Computer Physics Communications 244 (2019) 117–131. doi:10.1016/j.cpc.2019.06.013.

[39] P. Tsoutsanis, Stencil selection algorithms for WENO schemes on unstructured meshes, Journal of Computational Physics 475 (2023). doi:10.1016/j.jcp.2019.07.039.

[40] P. Tsoutsanis, X. Nogueira, L. Fu, A short note on a 3D spectral analysis for turbulent flows on unstructured meshes, Journal of Computational Physics 474 (2023). doi:10.1016/j.jcp.2022.111804.

[41] V. Maltsev, D. Yuan, K. Jenkins, M. Skote, P. Tsoutsanis, Hybrid discontinuous Galerkin-finite volume techniques for compressible flows on unstructured meshes, Journal of Computational Physics 473 (2023). doi:10.1016/j.jcp.2022.111755.

[42] D. Garmann, M. Visbal, P. Orkwis, Comparative study of implicit and subgrid-scale model large-eddy simulation techniques for low-Reynolds number airfoil applications, International Journal for Numerical Methods in Fluids 71 (12) (2013) 1546–1565.

[43] A. Beck, T. Bolemann, D. Flad, H. Frank, G. Gassner, F. Hindenlang, C.-D. Munz, High-order discontinuous Galerkin spectral element methods for transitional and turbulent flow simulations, International Journal for Numerical Methods in Fluids 76 (8) (2014) 522–548.

[44] B. Vermeire, F. Witherden, P. Vincent, On the utility of GPU accelerated high-order methods for unsteady flow simulations: A comparison with industry-standard tools, Journal of Computational Physics 334 (2017) 497–521.

[45] N. Simmonds, P. Tsoutsanis, A. Antoniadis, K. Jenkins, A. Gaylard, Low-Mach number treatment for finite-volume schemes on unstructured meshes, Applied Mathematics and Computation 336 (2018) 368–393. doi:10.1016/j.amc.2018.04.076.

[46] M. Galbraith, , M. Visbal, Implicit large eddy simulation of low Reynolds number flow past the SD7003 airfoil, 46th AIAA Aerospace Sciences Meeting and Exhibit (2008). doi:10.2514/6.2008-225.